The effects of the dielectric substrate thickness and the loss tangent on the absorption spectrum: a comprehensive study considering the resonance type, the ground plane coupling, and the characterization setup

UMUT KÖSE

EVREN EKMEKÇİ

Recommended Citation

The effects of the dielectric substrate thickness and the loss tangent on the absorption spectrum: a comprehensive study considering the resonance type, the ground plane coupling, and the characterization setup

Umut KÖSE[1,3]📷, **Evren EKMEKÇİ**[1,2,*]📷
[1]Department of Electronics and Communication Engineering, Süleyman Demirel University, Isparta, Turkey
[2]Department of Electrical and Electronics Engineering, Süleyman Demirel University, Isparta, Turkey
[3]Department of Electrical and Electronics Engineering, Fatih Sultan Mehmet Vakıf University,
İstanbul, Turkey

Abstract: In this study, the effects of dielectric substrate thickness and the dielectric loss tangent on the absorption spectrum are investigated parametrically in S-band. The study has been conducted on two different absorber topologies, one is closed ring resonator (CRR) and the other is composed of a split ring resonator (SRR), to observe the effects on both LC- and dipole-type resonances. The studies on the substrate thickness have been performed both numerically and experimentally, whereas the studies on the dielectric loss tangent have been performed numerically. The results agree with the literature such that the substrate thickness has significant effects on the resonant frequency and the absorption peak level which is explained by the impedance matching phenomenon. Besides, we show that the frequency shift behavior (i.e. redshift or blueshift) in response to substrate thickness change highly depends on the coupling between the resonator structure and the metallic ground plane. Moreover, the responses of absorption spectra to the changes of substrate thickness and dielectric loss are very similar whether it is due to an LC or a dipole-type resonances. We believe that the comprehensive and systematic parametric analyses in whole contributes to the literature especially considering the experimental studies in microwaves.

Key words: Metamaterial absorber, absorption peak level, LC resonance, dipole resonance, impedance matching

1. Introduction

Together with the increased trend on metamaterial studies [1–5], design and applications of metamaterial-based absorbers have become a popular research topic [7–52, 56, 57]. Therefore, a significant number of studies have been proposed on metamaterial based absorber designs at microwave [7–22, 25–28, 37–41], terahertz [23–25, 29–35, 43–51], far-infrared [42], midinfrared [25, 52], nearinfrared [25, 36, 56, 57], visible [25, 36] and ultraviolet [36] regions so far. Herein, the absorption (A) is defined by (1) [6–10, 14–20, 29–36].

$$A = 1 - |S_{11}|^2 - |S_{21}|^2 \ , \tag{1}$$

where $|S_{11}|^2$ is the reflectance and $|S_{21}|^2$ is the transmittance [6–10, 14–20, 29–36]. When the absorber is terminated by a metallic ground plane, the transmittance will be zero and the absorption will take a simpler

---

*Correspondence: evrenekmekci@sdu.edu.tr

form regarding only the reflectance terms as given in (2) [7–14, 22, 24, 29, 31–36].

$$A = 1 - |S_{11}|^2 \tag{2}$$

It should be borne in mind and be careful that both $|S_{11}|^2$ and $|S_{21}|^2$ may be composed of co- and crosspolarization terms depending on the absorber design [53–55].

In (1), the reflectance and transmittance values are desired to be eliminated to achieve highest possible absorption levels within the targeted frequency range. To eliminate the reflection, an impedance matching is performed between the metamaterial absorber and the propagation medium (i.e. mostly free-space) [8–11, 20–23, 25, 29–32, 35, 42, 43]. On the other hand, using a metallic ground plane at the bottom of the metamaterial structure is one of the most common ways in the literature to eliminate the transmission. This approach commonly yields a sandwiched structure composed of a metallic resonator, a dielectric substrate, and a metallic ground plane [7–21, 28–34, 40–46, 52–55]. Rather than using an all-metallic ground plane, there are some engineered approaches presented in the literature to eliminate transmissions such as taking the cumulative effects of both dielectric and magnetic losses together [47] or using an all-dielectric resonator with merged resonance modes which yield minimized reflectance and transmittance at the resonance region [6, 23, 27].

Within the scope of the studies to explain the working principles of resonator-based absorbers; there are a large number of articles in the literature considering the effects of the dielectric material losses on the absorption spectra [6, 12–17, 21–24, 31–33, 41–47]. Specifically, by considering their design, some of the studies conclude that increasing the dielectric loss increases the absorption level [14, 16, 41, 45–47], some of them state that the dielectric losses do not have significant effect on the absorption level [17, 22, 43, 44], another group of them demonstrate that increasing dielectric losses reduces the absorption level [13, 31, 33, 49], and the rest of them report that increasing dielectric losses increases the absorption level at the first stage than its further increase decreases the absorption level [6, 12, 15, 21, 23, 24, 26, 32, 42]. In addition to the dielectric loss, there are various reported findings regarding the effect of dielectric material thickness on the absorption spectrum [9–12, 17, 21, 25–29, 34, 35, 42–45, 50–52]. In more detail, references [9] and [17] present that the increase in dielectric material thickness decreases the absorption level, while references [9, 17, 25, 45, 52] present the opposite of this finding, i.e. they state that increasing dielectric material thickness increases the absorption level at the resonance frequency. Lastly, references [10–12, 21, 27–29, 34, 35, 39, 42, 50, 51] reveal that the absorption level increases with the dielectric thickness at the first stage and may decrease if the dielectric thickness increases further. On the other hand, if we consider the frequency behavior, increasing substrate thickness mostly reported to yield a redshift [10–12, 17, 28, 29, 34, 35, 42, 44, 50, 51] in the resonance frequency; however, there are some reported counterparts with blueshifts [10, 21, 39, 52]. To summarize the observations from the closely related literature, regarding the resonator-based absorber designs, Table 1 presents a detailed comparison table. The vast amount of the studies is conducted in a free-space medium and there are limited numbers of experimental work. The use of microwave waveguide setup along with the experimental studies distinguishes this study from the other studies discussed in Table 1. Considering the above discussed literature, we believe that this study contributes to the following aspects:

• A very early waveguide simulation results regarding only the CRR topology having different metallic design parameter values were presented in a national conference in Turkish by the same authors [21]. However, this study is a significantly extended version including newer design parameters, newer parametric substrate thickness values, experiments, literature comparison, comparing the waveguide simulation results with the

results obtained by free-space simulations, impedance calculations, and finally parametric analyses regarding the investigations of coupling between the resonator and the ground plane.

•We performed a series of numerical and experimental analysis in a rectangular waveguide medium on both closed ring resonator (CRR) and split ring resonator (SRR) based absorbers, separately to clarify the effects of substrate thickness and substrate losses on the absorption spectra. Studying CRR and SRR in the same study as a comparative way demonstrated that the responses of absorption spectra to the changes of substrate thickness and dielectric loss were very similar whether it was due to an LC or a dipole-type resonance. In this concept, including experimental analyses, especially by using a waveguide test environment in microwave, contributes to the literature.

•In the literature, the resonance frequency of the absorber mostly redshifts in response to the increased substrate thickness [10–12, 17, 28, 29, 34, 35, 42, 44, 50, 51]. There are limited number of studies that presents blueshift [10, 21, 39, 52]. In this study, we firstly presented blueshifts in both simulations and experiments for two different resonator topologies. Following, for our designs, we demonstrated with further analyses that the redshift/blueshift behavior is dependent on the coupling between the resonator and the ground plane.

2. Design

In this study, the designed metamaterial absorber structures consist of sandwich-type topology, which includes a metallic (i.e. copper) resonator at the top, a dielectric substrate in the middle and a full metallic ground plane at the bottom. As an illustration, a schematic side view of a sandwich-type absorber is demonstrated in Figure 1a. The absorber designs (i.e. CRR and SRR based absorbers) were realized by using Arlon AD300A laminate which had $t = 0.035$ mm thick copper (i.e. $\sigma_{cu} = 5.8 \times 10^7$ S/m) layers on both faces which sandwiched a d_{diel} thick dielectric layer whose dielectric constant was $\varepsilon_r = 3$ and dielectric loss tangent was $\tan \delta = 0.002$ at 10 GHz. Various numbers of d_{diel} values were studied to reveal the effect of the dielectric material thickness on the absorption. The studied d_{diel} values for the S-band waveguide analyses were 0.508 mm, 0.762 mm, 1.016 mm, 1.524 mm, and 2.540 mm for CRR based absorbers. On the other hand, they were 0.762 mm, 1.016 mm, 1.524 mm, 2.540 mm, and 3.048 mm for SRR based absorbers. Moreover, since it was not possible for us to find a specific type of substrate material with different dielectric loss tangent values physically (i.e. having same ε_r, same d_{diel} however different $\tan \delta$), the dielectric loss analyses had been conducted numerically by the choice of $\tan \delta$ as a variable.

The schematic top views and the design parameters of the CRR and SRR based sandwich-type absorbers are shown in Figures 1b and 1c, respectively. The design parameters and their corresponding values are tabulated in Table 2. Supporting, Figures 2a and 2b show the top view photographs of the fabricated CRR and SRR based S-band absorbers on various substrates, respectively. As an illustration, side view photographs of the fabricated CRR and SRR based absorbers are shown in Figures 2c and 2d, respectively. It is important to note here that during the conceptualization, deciding to work on two different resonator topologies (i.e. CRR and SRR) is mainly due to reveal the response of absorption spectrum to the changes in d_{diel} and $\tan \delta$ depending on the resonance type (i.e. LC or dipole resonance).

For the fabrication process, since we had Arlon AD300A with substrate thicknesses of 0.508 mm, 0.762 mm, 1.016 mm, and 1.524 mm available in our laboratory, the dielectric thickness of 2.540 mm was obtained by stacking two substrates with the thicknesses of 1.016 mm and 1.524 mm on top of each other. In more detail, the CRR or SRR which were formed on a 1.016-mm thick substrate without a metallic ground plane were attached to a 1.524-mm thick substrate having a blank top surface and a metallic ground plane at the bottom. The

Table 1. Comparison table regarding the closely related literature. In the absorption peak amplitude trend (Abs. Peak Amp. Trend) column: A refers that as the substrate thickness increases, the absorption peak first increases and then begins to decrease. B refers that as the substrate thickness increases, the absorption peak increases. C refers that as the substrate thickness increases, the absorption peak decreases. D refers that as the substrate loss increases, the absorption peak first increases and then begins to decrease. E refers that as the substrate loss increases, the absorption peak increases. F refers that as the substrate loss increases, the absorption peak decreases. Finally, G refers no significant change. In the absorption peak frequency trend (Abs. Peak Freq. Trend) column: As the substrate thickness increases, BS refers to blueshift, and RS refers to redshift.

Ref	Freq. region	Test setup	Resonator type	Substrate parameter under test (P: parametric)	Abs. Peak Amp. Trend	Abs. Peak Freq. Trend	Test method (Sim.: simulation Exp.: experiment, Int.: interference, TLM: transmission line model)
This work	µW	Waveguide	Metallic	Thickness (P)	A	BS	Sim., Exp.
				Loss (P)	D	-	Sim
[6]	µW	Waveguide	All-dielectric	Loss (P)	D	-	Sim.
[10]	µW	Free-space	Metallic	Thickness (P)	A	BS or RS	Sim.
[11]	µW	Free-space	Metallic	Thickness (P)	A	RS	Sim.
[12]	µW	Free-space	Metallic	Thickness (P)	A	RS	Sim.
				Loss (P)	D	-	Sim.
[13]	µW	Free-space	Metallic	Loss (P)	F	-	Sim.
[15]	µW	Free-space	Metallic	Loss (P)	D	-	Sim.
[17]	µW	Free-space	Metallic	Thickness (P)	B or C	RS	Sim.
				Loss (on/off)	G	-	Sim.
[21]	µW	Waveguide	Metallic	Thickness (P)	A	BS	Sim.
				Loss (P)	D	-	Sim.
[22]	µW	Free-space	Metallic	Loss (on/off)	G	-	Sim.
[23]	THz	Free-space	All-dielectric	Loss (P)	D	-	Sim., Exp.
[26]	µW	Free-space	Metallic	Loss (P)	D	-	Sim.
[27]	µW	Free-space	All-dielectric	Thickness (P)	A	-	Sim.
[28]	µW	Free-space	Metallic	Thickness (P)	A	RS	Sim.
[29]	THz	Free-space	Metallic	Thickness (P)	A	RS	Int. method
[31]	THz	Free-space	Metallic	Loss (P)	F	-	Sim.
[32]	THz	Free-space	Metallic	Loss (P)	D	-	Sim.
[33]	THz	Free-space	Metallic	Loss (P)	F	-	Sim.
[34]	THz	Free-space	Metallic	Thickness (P)	A	RS	Sim., Exp., Int. method
[35]	THz	Free-space	Metallic	Thickness (P)	A	RS	Int. method
[39]	µW	Free-space	Metallic	Thickness (P)	A	BS	Sim.
[41]	µW	Free-space	metallic	Loss (P)	E	-	Sim.
[42]	THz	Free-space	Metallic	Thickness (P)	A	RS	Sim., TLM
				Loss (P)	D	-	Sim., TLM
[43]	THz	Free-space	Metallic	Thickness (P)	G	-	Sim.
				Loss (on/off)	G	-	Sim.
[44]	THz	Free-space	Metallic	Thickness (P)	G	RS	Sim.
				Loss (on/off)	G	-	Sim.
[49]	THz	Free-space	Metallic	Loss (P)	F	-	Sim.
[50]	THz	Free-space	Metallic	Thickness (P)	A	RS	Sim., Exp., Int. method, TLM
[51]	THz	Free-space	Metallic	Thickness (P)	A	RS	Sim., Exp., Int. method
[52]	THz	Free-space	Metallic	Thickness (P)	B	BS	Sim.

attachment was performed by thin adhesive tapes at the edges to avoid air gaps in between the layers. A similar procedure was applied to obtain the dielectric thickness of 3.048 mm for the SRR case. Herein different than
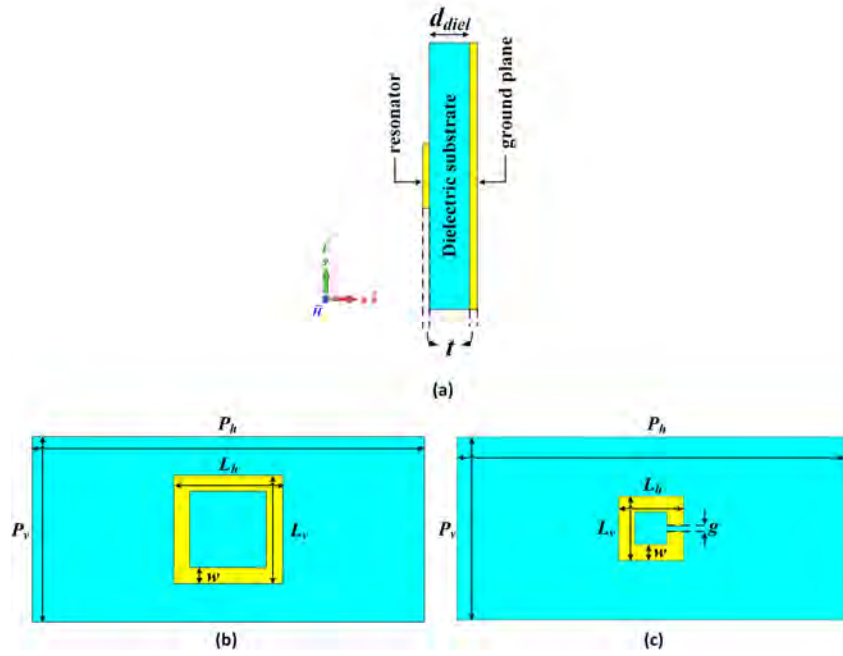
Figure 1. (a) A schematic side view of a sandwich-type absorber. Schematic top views and the design parameters of (b) CRR and (c) SRR based absorbers.

Table 2. The design parameters of the absorber structures.

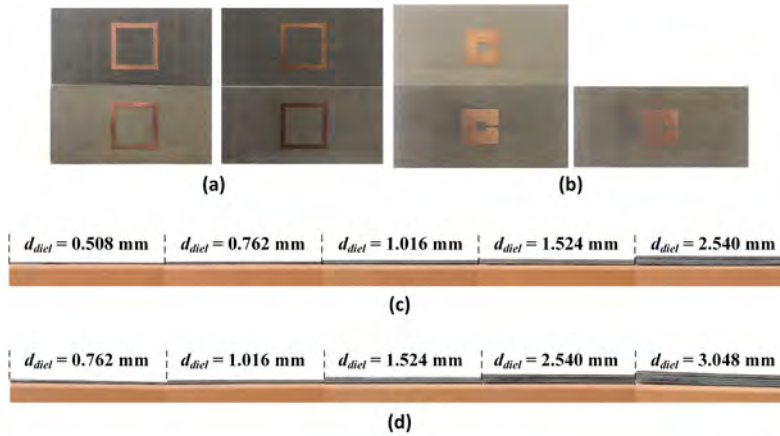| Structure	Design parameters (mm)					
	P_h	P_v	L_h	L_v	w	g
CRR	72	34.036	20	20.3	2.1	-
SRR	72	34.036	14	14.2	5.1	0.95

Figure 2. Photographs of the fabricated S-band structures with various dielectric thicknesses for the waveguide setup characterizations. (a) Top views of CRR based absorbers, (b) top views of SRR based absorbers, (c) side views of CRR based absorbers, and (d) side views of SRR based absorbers.

2.540-mm case, a 0.508-mm thick only dielectric layer, which was formed by removing the copper layers of 0.508 mm thick substrate on both faces, was sandwiched by the 1.016-mm and 1.524-mm thick dielectric layers. In

other words, the overall structure consisted of an SRR on a 1.016-mm thick dielectric, 0.508-mm thick dielectric, and finally a 1.524-mm thick dielectric with a metallic ground at the bottom. Like the 2.540-mm case, these separately fabricated layers were attached to each other by thin adhesive tapes at the edges. The effects of the adhesive tapes and the tiny interlayer air gaps which possibly occur due to the imperfect flatness of each layer were neglected in the simulations.

3. Simulation and experiment setups

In this study, the numerical analyses of the absorber designs were performed by CST Studio Suite® under frequency domain solver[1] by using either the S-band rectangular waveguide setup as shown in Figure 3a or the free-space setup based on the usage of unit-cell boundary conditions as shown in Figure 3b. The free-space setup uses unit-cell boundary conditions together with two floquet ports. This CST setup provides excitation of periodic structures by plane waves in free-space by using a unit-cell design [2]. On the other hand, the experimental analyses were conducted using an S-band waveguide setup (i.e. the experimental equivalent of the setup given in Figure 3a) whose photograph is shown in Figure 3c. Herein, two S-band rectangular hollow waveguide straights were connected to an Agilent FieldFox N9926A vector network analyser through WR-284 coaxial-to-waveguide adapters at each end. During the measurements, the absorber structures were placed in the 28.6-mm long sample holder (i.e. $\lambda/4$ spacer). A larger photograph of the sample holder is shown in Figure 3d where a CRR based absorber unit cell was placed as an example. The measurement setup was calibrated by using the thru-reflect-line (TRL) calibration technique where the edges of the sample holder were set as the reference planes.
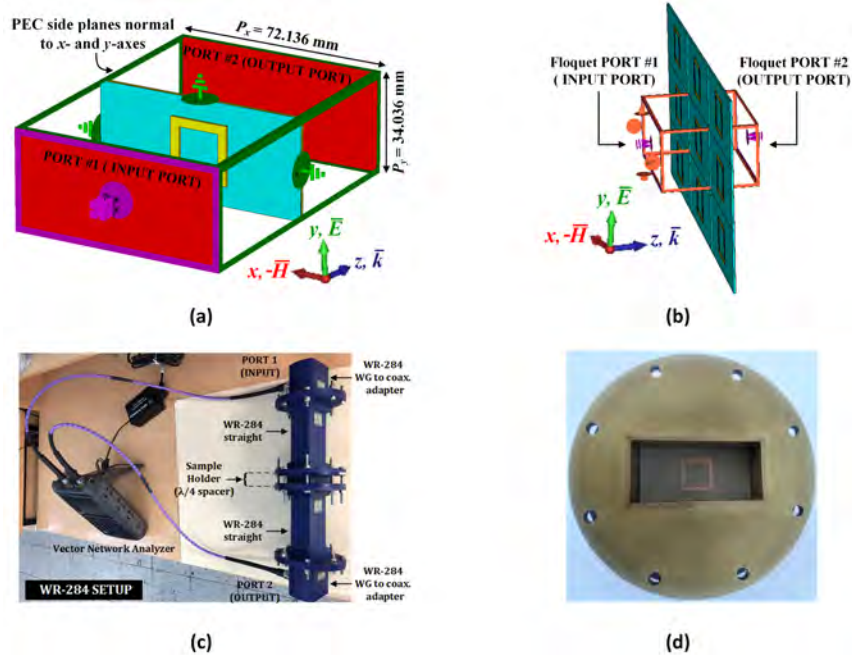

Figure 3. (a) The CST Studio Suite S-band waveguide simulation setup. (b) The CST Studio Suite free-space simulation setup by using unit-cell boundaries. (c) WR-284 experiment setup. (d) Absorber unit-cell in S-band sample holder.

---

[1]CST Studio Suite®, Dassault Systèmes, the 3DEXPERIENCE® Company (online) Website https://www.3ds.com/products-services/simulia/products/cst-studio-suite/ [accessed 16 April 2022].

[2]foot1

In both the rectangular waveguide simulations and experiments, the structures were excited by fundamental TE_{10} mode, where the propagation vector $\vec{k}$ was along z axis, the electric field vector $\vec{E}$ was along y axis and magnetic field vector $\vec{H}$ was approximated to be only along x axis, since z components of the $\vec{H}$ field did not play a crucial role in the excitation of the resonator, due to the fact that the resonator was placed in the middle of the waveguide crosssection [1, 2, 6, 16, 18, 19]. On the other hand, in the free-space simulations, the structures were excited by plane waves [3]. For the copolarization excitations the propagation vector $\vec{k}$ was along z axis, the electric field vector $\vec{E}$ was along y axis, and magnetic field vector $\vec{H}$ was along x axis.

4. Results

4.1. Effects of dielectric material thickness on the absorption spectrum

The simulation and the experiment results of CRR and SRR based absorbers by using rectangular waveguide setups for various d_{diel} values are shown in Figure 4. For all cases, it has been observed that f_0 increases as d_{diel} gets higher. In addition, the absorption peak value firstly tends to increase as d_{diel} increases from 0.508 mm to 1.016 mm then it starts to decrease dramatically as d_{diel} gets higher values for the CRR based absorber case (see Figures 4a and 4b). Moreover, the absorption peak value becomes almost unity at 2.801 GHz in simulations and at 2.826 GHz in experiments when $d_{diel} = 1.016$ mm. On the other hand, a very similar behavior is observed for SRR based absorber as shown in Figures 4c and 4d. For this case, the absorption peak value starts to increase as d_{diel} increases from 0.762 mm to 1.524 mm then it tends to decrease dramatically as d_{diel} increases. Finally, the absorption peak value for this case becomes almost unity for $d_{diel} = 1.524$ mm at 3.134 GHz in simulations and at 3.146 GHz in experiments.
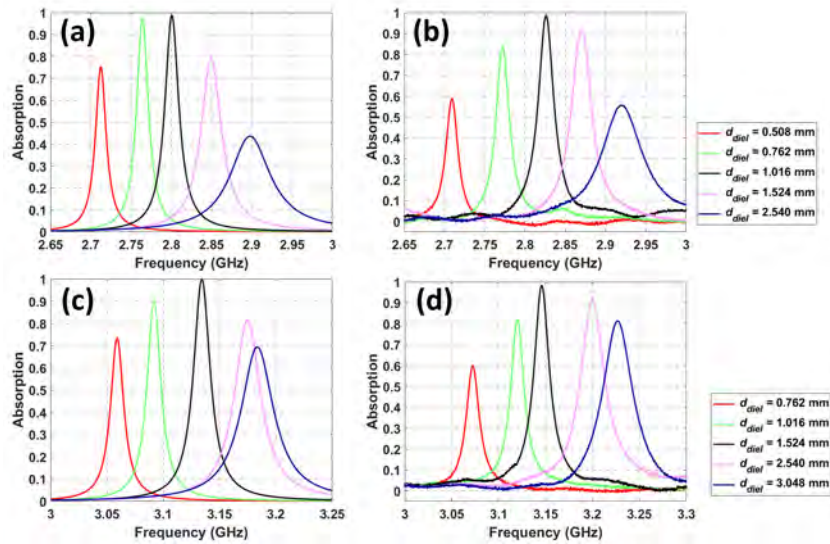

Figure 4. The absorption spectra of the S-band structures obtained for different dielectric thicknesses by the waveguide setups. (a) CRR based absorber simulation, (b) CRR based absorber experiment, (c) SRR based absorber simulation, and (d) SRR based absorber experiment.

The behavior which is observed from the simulation and the experiment results are very similar. In terms of f_0, the highest percentage error between the experimental and the simulation results is only 0.89% for

---

[3]foot1

CRR based absorbers, and 1.35% for SRR based absorbers. These percentage errors and the other affordable discrepancies observed on the spectra may be due to fabrication errors (i.e. imperfect resonator dimensions), nonideal material electric and dielectric properties, tiny air gaps between dielectric layers which may possibly occur in the layered designs (i.e. 2.540 mm and 3.048 mm thick dielectric cases) and possible imperfections in the experimental setup.

In Figure 4, the dependence of absorption peak value on d_{diel} may be explained by the impedance matching mechanism. To do that the normalized impedance $\tilde{z}(\omega)$ can be calculated by (3) [5, 24, 45, 48].

$$\tilde{z}(\omega) = \sqrt{\frac{(1 + S_{11})^2 - (S_{21})^2}{(1 - S_{11})^2 - (S_{21})^2}} \qquad (3)$$

As we have a complete metallic ground in our design, S_{21} term will be zero, therefore (3) will take a simpler form as given in (4) [24, 48].

$$\tilde{z}(\omega) = \frac{(1 + S_{11})}{(1 - S_{11})} \qquad (4)$$

Based on (4), the complex normalized impedances of the absorbers regarding the waveguide simulation results are presented in Figures 5a and 5b for CRR based absorbers and in Figures 5c and 5d for SRR based absorbers. Figure 5 reveals that changing the substrate thickness affects $\tilde{z}(\omega)$ significantly which means that the impedance matching between the guiding medium and the absorber structure is affected. Therefore, different levels of absorption values are observed in Figure 4 due to the change in substrate thickness.
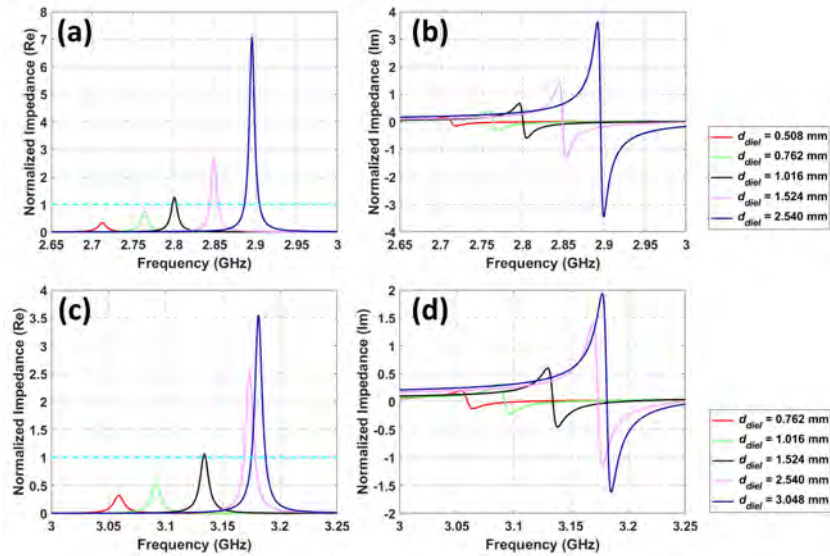

Figure 5. The complex normalized impedances for several dielectric thicknesses calculated by the S-parameters obtained by waveguide simulation setup. (a) Real part for CRR based absorber, (b) imaginary part for CRR based absorber, (c) real part for SRR based absorber, and (d) imaginary part for SRR based absorber.

4.2. Effects of dielectric material loss on the absorption spectrum

To complete the picture, the effects of the dielectric material loss tangent (i.e. $\tan\delta$) on the absorption spectrum have been studied considering the substrate thickness d_{diel} and the resonator type. On this aim, the absorption spectra have been numerically calculated at seven different values of $\tan\delta$, ranging from 0 to 0.04, with three different d_{diel} values for each resonator type (i.e. d_{diel} = 0.762 mm, 1.016 mm, and 1.524 mm for CRR based absorber and d_{diel} = 1.016 mm, 1.524 mm, and 2.540 mm for SRR based absorber). The results are given in Figure 6. As the main observation, f_0 is not significantly affected by the change of $\tan\delta$, however the absorption peak level is. In more detail, among the $\tan\delta$ values under investigation, CRR based absorbers get their highest absorption levels (i.e. almost unity) for $\tan\delta$ values that are 0.0015, 0.0015, and 0.0065 with d_{diel} values that are 0.762 mm, 1.016 mm, and 1.524 mm, respectively. Similarly, SRR based absorbers reach almost unity absorption levels for $\tan\delta$ values that are 0, 0.0015 and 0.0065 with d_{diel} values that are 1.016 mm, 1.524 mm, and 2.540 mm, respectively. Moreover, the absorption peak levels do not take their minimum values as $\tan\delta$ reaches to 0.04 value for all cases. This is an important indicator showing that the absorption peak level is not always directly proportional with $\tan\delta$.
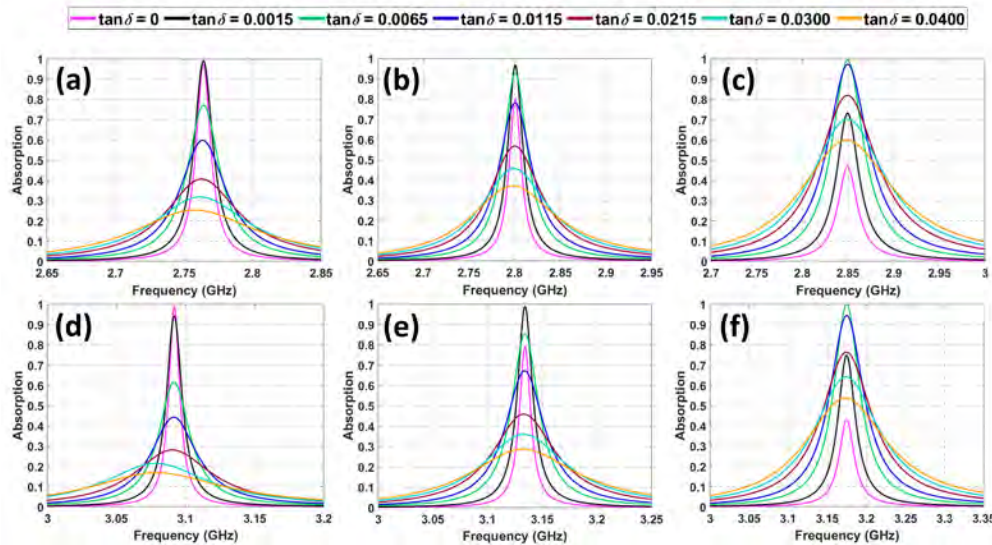

Figure 6. Absorption spectra of several designs depending on $\tan\delta$ obtained by waveguide simulations. (a) CRR based absorber for d_{diel} 0.762 mm, (b) CRR based absorber for d_{diel} 1.016 mm, (c) CRR based absorber for d_{diel} 1.524 mm, (d) SRR based absorber for d_{diel} 1.016 mm, (e) SRR based absorber for d_{diel} 1.524 mm, (f) SRR based absorber for d_{diel} 2.540 mm.

One of the outcomes of this study is to demonstrate that the behavior observed in the absorption spectrum is not dependent on whether the resonance type is an LC or a dipole. In literature SRR type resonators are commonly used to excite LC type resonances [3, 4, 40] and CRR type resonators are used to excite electrical dipole resonances [14, 16, 46]. To support these findings, the surface current plots on the SRR (d_{diel} = 1.524 mm and $\tan\delta$ = 0.002) and the CRR (d_{diel} = 1.016 mm and $\tan\delta$ = 0.002) based absorbers at their resonance frequencies are plotted in Figure 7 by using waveguide simulation setup. In Figure 7a, two parallel current flows having same directions are obviously observed at the vertical arms of the CRR which indicates the presence of a dipole resonance [14, 16, 46, 49]. On the other hand, the circulating current density along the SRR plane in Figure 7b reveals the existence of the excited LC resonance [3, 4, 40, 49]. In both CRR and SRR cases,

the surface current densities on the resonator plane and the corresponding surface current densities on the ground plane are in opposite directions. It has been reported in literature that these opposite current densities constitute magnetic dipoles [14, 19, 31, 35].
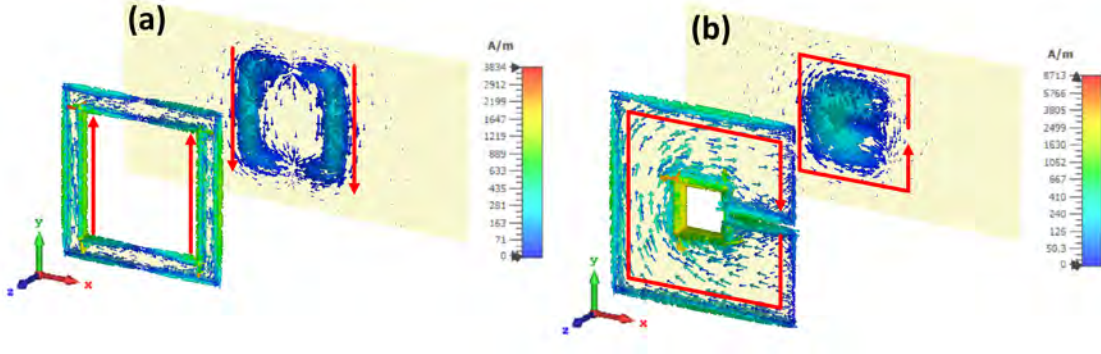

Figure 7. The surface current plots on (a) CRR ($d_{diel} = 1.016$ mm and $\tan\delta = 0.002$) and (b) SRR ($d_{diel} = 1.524$ mm and $\tan\delta = 0.002$) based absorbers at their resonance frequencies obtained by waveguide simulation setup.

4.3. Effects of ground plane coupling on the absorption spectrum

An important part of the close literature reports redshifts in the resonance frequencies in response to increased substrate thickness [11, 12, 17, 28, 29, 34, 35, 42, 44, 50, 51]. However, albeit limited, there are also studies that report blueshift supporting our findings [10, 39, 52]. To clarify this difference, we studied on the CRR and SRR based absorbers adhering to the design parameters given in Table 2, however by using much thicker substrate thicknesses to reduce the ground coupling effect [51, 58, 59]. The numerical analyses were performed by using the same waveguide simulation setup (see Figure 3a) in CST. The relevant results given in Figure 8 reveal the systematic redshifts with the increased substrate thicknesses, supporting the results given in [11, 12, 17, 28, 29, 34, 35, 42, 44, 50, 51]. In addition, Figure 9 reveals the reduced or negligible coupling between the resonators and the ground plane. Different than Figure 7, the opposite current distributions observed in the ground plane are disappeared. Moreover, no significant current distribution related to the coupling is observed. Therefore, it has been evaluated that the reason of the blueshifts in Figure 4 is the coupling which occur between the resonator structure and the ground plane.
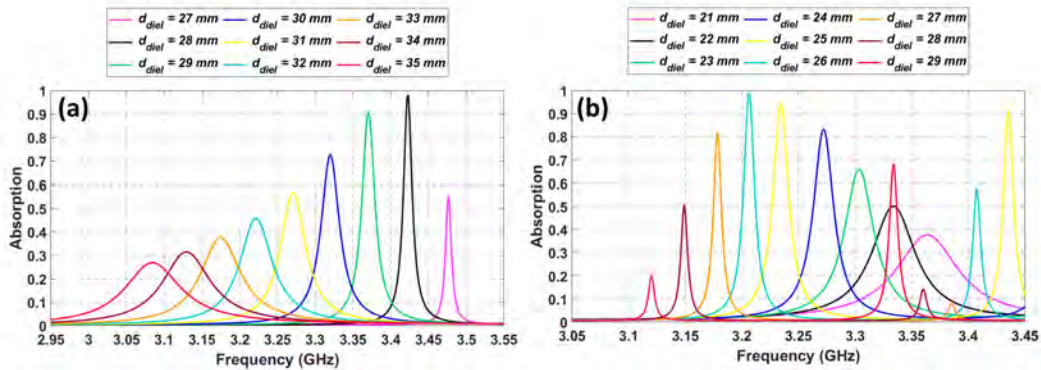

Figure 8. The absorption spectra of the resized (a) CRR and (b) SRR structures with increased substrate thicknesses (d_{diel}) obtained by waveguide simulation setup.
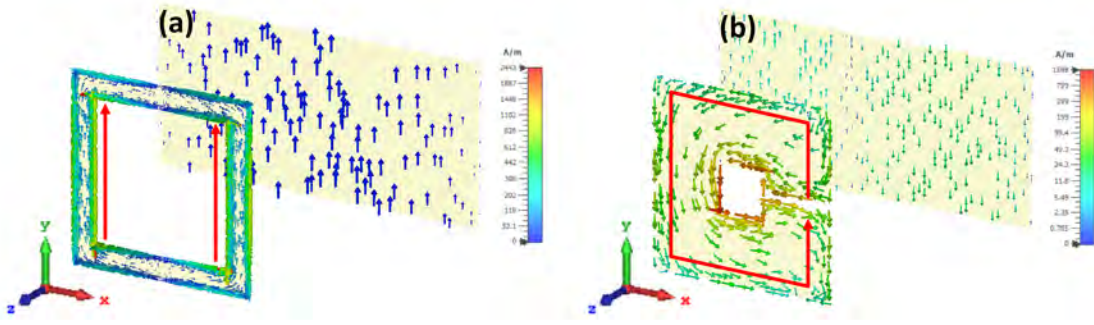
Figure 9. The surface current plots on (a) CRR ($d_{diel} = 29$ mm and $\tan\delta = 0.002$) and (b) SRR ($d_{diel} = 26$ mm and $\tan\delta = 0.002$) based absorbers at their resonance frequencies obtained by waveguide simulation setup.

4.4. Comparison of the waveguide and free-space simulation results

The main characterizations in this study were performed by using an S-band rectangular waveguide setup. As the main advantages, the waveguide setup enables us to simulate an array behavior by using a unit-cell structure and it does not need an anechoic chamber environment [53]. However, the waveguide setup does not support a plane wave propagation [60]. On the other hand, placing the design in the middle of the waveguide crosssection is expected to reduce the effects of longitudinal H-field components in TE_{10} mode of excitation [53]. Nevertheless, we compared the results obtained by the rectangular waveguide setup (Figure 3a) and free-space setup (Figure 3b) for both SRR and CRR structure as presented in Figure 10. The results show that the waveguide and free-space results are very consistent. The small discrepancies are thought to be due to the excitation signal differences, where in the waveguide setup a TE_{10} mode is used and in the free-space setup the plane wave excitation is used.
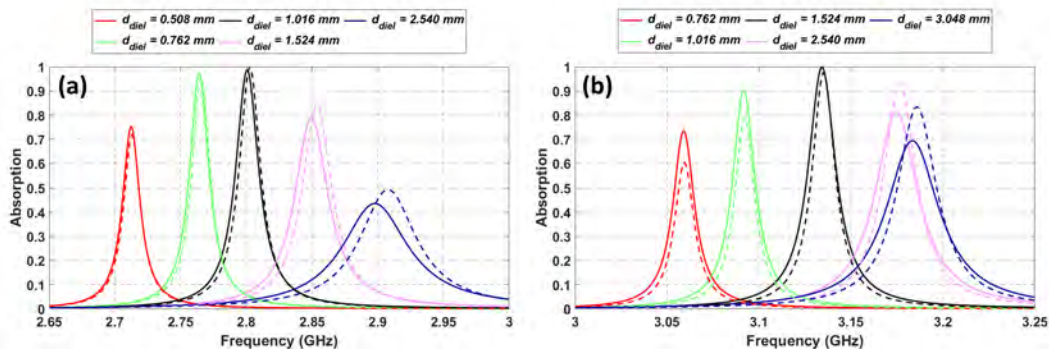

Figure 10. The comparison of the waveguide results with that of free-space results in simulations for (a) CRR and (b) SRR based absorbers having several substrate thicknesses (d_{diel}). Where, solid, and dashed lines belong to the results for waveguide and free-space simulations, respectively.

Investigation of the effects of crosspolarization reflection in addition to copolarized reflection is possible with CST floquet port excitation by using the first two modes [4]. Here we want to note that the crosspolarization reflections are practically zero in both CRR and SRR designs depending on the CST simulations.

---

[4]foot1

5. Conclusion

In this study, detailed parametrical analyses were performed to reveal the effects of substrate parameters (i.e. substrate thickness and substrate loss tangent) on the absorption spectrum of CRR and SRR based absorbers in S-band. The results show that the choice of substrate thickness, without changing its loss tangent, is not only effective on f_0 but also on the absorption peak level. These substrate thickness analyses have been supported by complex impedance plots, where the real parts of the normalized impedances are nearly unity at the cases where the maximum absorption are obtained. This observation comes together with a design flexibility that a perfect absorption may be possible by tuning the substrate material properties rather than tuning metallic resonator design parameters. Specifically, almost perfect absorptions have been obtained for CRR and SRR based absorbers for the substrate thicknesses 1.016 mm and 1.524 mm, respectively. On the other hand, it has been shown that the coupling between the resonator and the metallic ground plane has an important effect on the shift behavior of the resonance frequency. In more detail, for both CRR and SRR structure, a blueshift behavior was observed for the lower substrate thicknesses where the coupling between the resonator and the ground plane was effective and a redshift behavior was observed for the higher substrate thicknesses where the coupling between the resonator and the ground plane was neglected. Moreover, it has been presented that the response of the absorption spectra on the changes of substrate thickness and substrate loss tangent are very similar regardless of whether the resonance is LC-or a dipole-type. Lastly, it has been shown that the waveguide simulations results are very consistent with the unit-cell free-space simulation setup, for our design. It is believed that the results fill a gap in the literature and are useful especially for metamaterial or resonator-based absorber designs.

References

[1] Ekmekci E, Turhan-Sayan G. Multi-functional metamaterial sensor based on a broad-side coupled SRR topology with a multi-layer substrate. Applied Physics A 2013; 110 (1): 189–197. doi:10.1007/s00339-012-7113-1

[2] Ekmekci E, Kose U, Cinar A, Ertan O, Ekmekci Z. The Use of Metamaterial type double-sided resonator structures in humidity and concentration sensing applications. Sensors and Actuators A: Physical 2019; 297: 111559. doi:10.1016/j.sna.2019.111559

[3] Seliuta D, Zimkaite D, Slekas G, Urbanovic A, Devenson J et al. Optimization of modulation properties of terahertz metamaterial by tuning Fabry–Pérot resonances. IEEE Transactions on Terahertz Science and Technology 2014; 5 (1): 1–7. doi:10.1109/TTHZ.2014.2367240

[4] Chen ZC, Han NR, Pan ZY, Gong YD, Chong TC et al. Tunable resonance enhancement of multi-layer terahertz metamaterials fabricated by parallel laser micro-lens array lithography on flexible substrates. Optical Materials Express 2011; 1 (2): 151. doi:10.1364/OME.1.000151

[5] Smith DR, Vier DC, Koschny T, Soukoulis CM. Electromagnetic parameter retrieval from inhomogeneous metamaterials. Physical Review E 2005; 71(3): 1–11. doi:10.1103/PhysRevE.71.03661

[6] Karacan N, Ekmekci E. An all-dielectric microwave absorber composed of a dielectric hollow cylinder filled by chemical liquids and its application on sensing. Sensors and Actuators A: Physical 2020; 314: 112235. doi:10.1016/j.sna.2020.112235

[7] Wanghuang T, Chen W, Huang Y, Wen G. Analysis of metamaterial absorber in normal and oblique incidence by using interference theory. AIP Advances 2013; 3 (10). doi:10.1063/1.4826522

[8] Bagci F, Medina E. Design of a wide-angle, polarization-insensitive, dual-band metamaterial-inspired absorber with the aid of equivalent circuit model. Journal of Computational Electronics 2017; 16 (3): 913–921. doi:10.1007/s10825-017-1009-4

[9] Kim SJ, Yoo YJ, Kim YJ, Lee YP. Triple-band metamaterial absorption utilizing single rectangular hole. Optics Communications 2017; 382: 151–156. doi:10.1016/j.optcom.2016.07.075

[10] Ji S, Jiang C, Zhao J, Zhang X, He Q. Design of a polarization-insensitive triple-band metamaterial absorber. Optics Communications 2019; 432: 65–70. doi:10.1016/j.optcom.2018.09.040

[11] Cheng Y, Nie Y, Gong R. Metamaterial absorber and extending absorbance bandwidth based on multi-cross resonators. Applied Physics B 2013; 111 (3): 483–488. doi:10.1007/s00340-013-5361-1

[12] Wang AX, Qu SB, Yan M, Wang WJ, Wang J et al. Six-band polarization-insensitive perfect metamaterial absorber using L-shaped resonators. Applied Physics A 2019; 125 (5): 331. doi:10.1007/s00339-019-2568-y

[13] Zhong J, Huang Y, Wen G, Sun H, Wang P et al. Single-/dual-band metamaterial absorber based on cross-circular-loop resonator with shorted stubs. Applied Physics A: Materials Science and Processing 2012; 108 (2): 329–335. doi:10.1007/s00339-012-6989-0

[14] Shen X, Cui TJ, Zhao J, Ma HF, Jiang WX et al. Polarization-independent wide-angle triple-band metamaterial absorber. Optics Express 2011; 19 (10): 9401. doi:10.1364/oe.19.009401

[15] Hu C, Li X, Feng Q, Chen X, Luo X. Investigation on the role of the dielectric loss in metamaterial absorber. Optics Express 2010; 18 (7): 6598. doi:10.1364/oe.18.006598

[16] Ekmekci E, Demir E. On/Off switching of absorption spectra by layer shifting for double-layer metamaterial-based absorber. IEEE Antennas and Wireless Propagation Letters 2016; 15: 532–535. doi:10.1109/LAWP.2015.2457091

[17] Wang Q, Cheng Y. Compact and low-frequency broadband microwave metamaterial absorber based on meander wire structure loaded resistors. AEU - International Journal of Electronics and Communications 2020; 120: 153198. doi:10.1016/j.aeue.2020.153198

[18] Al-Badri KSL, Cinar A, Kose U, Ertan O, Ekmekci E. Monochromatic tuning of absorption strength based on angle-dependent closed-ring resonator-type metamaterial absorber. IEEE Antennas and Wireless Propagation Letters 2017; 16: 1060–1063. doi:10.1109/LAWP.2016.2620599

[19] Al-Badri KSL, Karacan N, Kucukoner EM, Ekmekci E. Sliding planar conjoined cut-wire-pairs: A novel approach for splitting and controlling the absorption spectra. Journal of Applied Physics 2018; 124 (10): 105103. doi:10.1063/1.5040927

[20] Landy NI, Sajuyigbe S, Mock JJ, Smith DR, Padilla WJ. Perfect metamaterial absorber. Physical Review Letters 2008; 100 (20). doi:10.1103/PhysRevLett.100.207402

[21] Köse U, Ekmekçi E. Metamalzeme tabanlı soğurucu yüzeylerde soğurma miktarının dielektrik malzeme özelliğine göre nümerik olarak incelenmesi. In: IX. URSI-Türkiye Bilimsel Kongresi, Konya, Türkiye; 2018 (in Turkish).

[22] Zhao J, Cheng Y. Ultrabroadband microwave metamaterial absorber based on electric SRR loaded with lumped resistors. Journal of Electronic Materials 2016; 45(10): 5033–5039. doi:10.1007/s11664-016-4693-0

[23] Cardin A, Fan K, Padilla W. Role of loss in all-dielectric metasurfaces. Optics Express 2018; 26 (13): 17669. doi:10.1364/oe.26.017669

[24] He XJ, Wang Y, Wang JM, Gui TL, Wu Q. Dual-band terahertz metamaterial absorber with polarization insensitivity and wide incident angle. Progress in Electromagnetics Research 2011; 115: 381–397. doi:10.2528/PIER11022307

[25] Watts CM, Liu X, Padilla WJ. Metamaterial electromagnetic wave absorbers. Advanced Materials 2012; 24 (23): OP98–OP120. doi:10.1002/adma.201200674

[26] Sellier A, Teperik T, V de Lustrac T. V. Resonant circuit model for efficient metamaterial absorber. Optics Express 2013; 21 (106): A997. doi:10.1364/OE.21.00A997

[27] Xie J, Quader S, Xiao F, He C, Liang X et al. Truly all-dielectric ultrabroadband metamaterial absorber: Water-based and ground-free. IEEE Antennas and Wireless Propagation Letters 2019; 18 (3): 536–540. doi:10.1109/LAWP.2019.2896166

[28] Xiong H, Yu YT, Tang MC, Chen SY, Liu DP et al. Varied absorption peaks of dual-band metamaterial absorber analysis by using reflection theory. Applied Physics A 2016; 122 (3): 164. doi:10.1007/s00339-016-9704-8

[29] Duan G, Schalch J, Zhao X, Li A, Chen C et al. A survey of theoretical models for terahertz electromagnetic metamaterial absorbers. Sensors and Actuators A: Physical 2019; 287: 21–28. doi:10.1016/j.sna.2018.12.039

[30] Tao H, Landy NI, Bingham CM, Zhang X, Averitt RD et al. A metamaterial absorber for the terahertz regime: Design, fabrication and characterization. Optics Express 2008; 16 (10): 7181. doi:10.1364/oe.16.007181

[31] Astorino MD, Frezza F, Tedeschi N. Ultra-thin narrow-band, complementary narrow-band, and dual-band metamaterial absorbers for applications in the THz regime. Journal of Applied Physics 2017; 121 (6): 063103. doi:10.1063/1.4975687

[32] Tao H, Bingham CM, Pilon D, Fan K, Strikwerda AC et al. A dual band terahertz metamaterial absorber. Journal of Physics D: Applied Physics 2010; 43 (22): 225102. doi:10.1088/0022-3727/43/22/225102

[33] Astorino MD, Frezza F, Tedeschi N. Broad-band terahertz metamaterial absorber with stacked electric ring resonators. Journal of Electromagnetic Waves and Applications 2017; 31 (7): 727–739. doi:10.1080/09205071.2017.1308839

[34] Huang L, Chowdhury DR, Ramani S, Reiten MT, Luo SN et al. Impact of resonator geometry and its coupling with ground plane on ultrathin metamaterial perfect absorbers. Applied Physics Letters 2012; 101 (10): 1–9. doi:10.1063/1.4749823

[35] Chen HT. Interference theory of metamaterial perfect absorbers. Optics Express 2012; 20 (7): 7165. doi:10.1364/oe.20.007165

[36] Qi B, Zhao Y, Niu T, Mei Z. Ultra-broadband metamaterial absorber based on all-metal nanostructures. Journal of Physics D: Applied Physics 2019; 52 (42): 425304. doi:10.1088/1361-6463/ab31ff

[37] Li W, Zhang Y, Wu T, Cao J, Chen Z et al. Broadband radar cross section reduction by in-plane integration of scattering metasurfaces and magnetic absorbing materials. Results in Physics 2019; 12: 1964–1970. doi:10.1016/j.rinp.2019.01.080

[38] Jeong H, Kim Y, Tentzeris MM, Lim S. Gain-enhanced metamaterial absorber-loaded monopole antenna for reduced radar cross-section and back radiation. Materials 2020; 13 (5): 1247. doi:10.3390/ma13051247

[39] Li MH, Liu SY, Guo LY, Lin H, Yang HL et al. Influence of the dielectric-spacer thickness on the dual-band metamaterial absorber. Optics Communications 2013; 295: 262–267. doi:10.1016/j.optcom.2013.01.030

[40] Fu X, Zeng X, Cui TJ, Lan C, Guo Y et al. Mode jumping of split-ring resonator metamaterials controlled by high-permittivity BST and incident electric fields. Scientific Reports 2016; 6 (1): 31274. doi:10.1038/srep31274

[41] Tuong PV, Park JW, Lam VD, Jang WH, Nikitov SA et al. Dielectric and ohmic losses in perfectly absorbingmetamaterials. Optics Communications 2013; 295: 17–20. doi:10.1016/j.optcom.2013.01.031.

[42] Costa F, Genovesi S, Monorchio A, Manara G. A circuit-based model for the interpretation of perfect metamaterial absorbers. IEEE Transactions on Antennas and Propagation 2013; 61 (3): 1201–1209. doi:10.1109/TAP.2012.2227923

[43] Pan W, Yu X, Zhang J, Zeng W. A broadband terahertz metamaterial absorber based on two circular split rings. IEEE Journal of Quantum Electronics 2017; 53 (1): 1–6. doi:10.1109/JQE.2016.2643279

[44] Hu D, Wang H, Tang Z, Zhang X. Investigation of a broadband refractory metal metamaterial absorber at terahertz frequencies. Applied Optics 2016; 55 (19): 5257. doi:10.1364/ao.55.005257

[45] Hu D, Wang H, Tang Z, Zhang X, Zhu Q. Design of four-band terahertz perfect absorber based on a simple #-shaped metamaterial resonator. Applied Physics A 2016; 122 (9): 826. doi:10.1007/s00339-016-0357-4

[46] Wang BX, Wang LL, Wang GZ, Huang WQ, Li XF et al. A Broadband, polarisation-insensitive and wide-angle coplanar terahertz metamaterial absorber. The European Physical Journal B 2014; 87 (4): 98. doi:10.1140/epjb/e2014-41072-y

[47] Landy NI, Bingham CM, Tyler T, Jokerst N, Smith DR et al. Design, theory, and measurement of a polarization-insensitive absorber for terahertz imaging. Physical Review B 2009; - Condensed Matter and Materials Physics 79 (12): 1–6. doi:10.1103/PhysRevB.79.125104

[48] Du X, Yan F, Wang W, Tan S, Zhang L et al. A polarization- and angle-insensitive broadband tunable metamaterial absorber using patterned graphene resonators in the terahertz band. Optics & Laser Technology 2020; 132: 106513. doi:10.1016/j.optlastec.2020.106513

[49] Duan G, Schalch J, Zhao X, Zhang J, Averitt RD et al. An air-spaced terahertz metamaterial perfect absorber. Sensors and Actuators A: Physical 2018; 280: 303–308. doi:10.1016/j.sna.2018.07.052

[50] Duan G, Schalch J, Zhao X, Zhang J, Averitt RD et al. Identifying the perfect absorption of metamaterial absorbers. Physical Review B 2018; 97 (3): 035128. doi:10.1103/PhysRevB.97.035128

[51] Duan G, Schalch J, Zhao X, Zhang J, Averitt RD et al. Analysis of the thickness dependence of metamaterial absorbers at terahertz frequencies. Optics Express 2018; 26 (3): 2242. doi:10.1364/oe.26.002242

[52] Liao YL, Zhao Y. A wide-angle broadband polarization-dependent absorber with stacked metal-dielectric grating. Optics Communications 2016; 370: 245–249. doi:10.1016/j.optcom.2016.03.033.

[53] Karacan N, Ekmekci E, Turhan-Sayan G. Response to "Comment on 'Sliding Planar Conjoined Cut-Wire-Pairs: A Novel Approach for Splitting and Controlling the Absorption Spectra'" [J. Appl. Phys. 128, 126101 (2020)]. Journal of Applied Physics 2020; 128 (12): 1–5. doi:10.1063/5.0018386

[54] Kundu D, Mohan A, Chakrabarty A. Reduction of cross-polarized reflection to enhance dual-band absorption. Journal of Applied Physics 2016; 120 (20). doi:10.1063/1.4968569.

[55] Kundu D, Baghel S, Mohan A, Chakrabarty A. Design and analysis of printed lossy capacitive surface-based ultrawideband low-profile absorber. IEEE Transactions on Antennas and Propagation 2019; 67 (5): 3533–3538. doi:10.1109/TAP.2019.2902660

[56] Zhong Q, Wang T, Jiang X, Cheng L, Yan R et al. Near-infrared multi-narrowband absorber based on plasmonic nanopillar metamaterial. Optics Communications 2020; 458: 124637. doi:10.1016/j.optcom.2019.1247

[57] Alici KB, Turhan AB, Soukoulis CM, Ozbay E. Optically thin composite resonant absorber at the near-infrared band: A polarization independent and spectrally broadband configuration. Optics Express 2011; 19 (15): 14260. doi:10.1364/oe.19.014260

[58] Tretyakov SA, Simovski CR. Dynamic model of artificial reactive impedance surfaces. Journal of Electromagnetic Waves and Applications 2003; 17 (1): 131–145. doi:10.1163/156939303766975407

[59] Ma S, Xiao S, Zhou L. Resonant modes in metal/insulator/metal metamaterials: An analytical study on near-field couplings. Physical Review B 2016; 93 (4): 1–11. doi:10.1103/PhysRevB.93.045305

[60] Pozar DM. Microwave Engineering. 4th ed. John Wiley & Sons, Inc, 2011.